Hindawi
Journal of Spectroscopy
Volume 2020, Article ID 2521696, 8 pages
https://doi.org/10.1155/2020/2521696

Research Article

Sparse Representation for Different Animal Vertebra Classification along the Fixation Trajectory of Pedicle Screw

YangYang Liu,[1,2] ZhiQiang Wang,[3] Kang Wang,[1] ZhiYu Qian,[1] Yang Gao,[2] and WeiTao Li[1]

[1]*Nanjing University of Aeronautics and Astronautics, Department of Biomedical Engineering, Nanjing 211106, China*
[2]*Nanjing Institute of Technology, College of Information and Communication Engineering, Nanjing 211167, China*
[3]*Nanjing University of Posts and Telecommunications, School of Communication and Information Engineering, Nanjing 210003, China*

Correspondence should be addressed to WeiTao Li; liweitao@nuaa.edu.cn

Received 4 July 2019; Revised 1 September 2019; Accepted 10 September 2019; Published 20 January 2020

Academic Editor: Young Jong Lee

Pedicle screw (PS) implantation is an ideal method for the treatment of severe multilevel vertebral instability. The key problem is the accuracy of PS fixation. In this paper, the spectrum of different tissues along the fixation trajectory of PS is studied to tackle the accuracy problem. Fresh porcine vertebrae, bovine vertebrae, and ovine vertebrae were measured by using the near-infrared spectrum (NIRs) device to obtain the reflected spectrum from these vertebrae. Along the fixation trajectory of PS, the classification method based on the sparse representation-based classifier (SRC) was applied to different vertebral tissues (cortical bones and cancellous bones). Considering the large amount of spectral data, sparse preserving projection (SPP) was applied to improve the performance of SRC. The proposed method based on the SPP method for dimensionality reduction and the SRC method for tissue recognition was first used in vertebrae classification and showed superior performance compared with other classification methods, such as SVM and 1NN. The results gained from this project are vital significant to the development of hi-tech medical instruments with independent intellectual property rights.

1. Introduction

Pedicle screw (PS) implantation is an ideal method for the treatment of severe multilevel vertebral instability [1–4]. Accuracy in placement of PS is very important for effective PS fixation, which has attracted extensive interest in increasing the accuracy of tissue recognition and PS placement [5–8]. Nowadays postoperative computed tomography (CT) scan becomes the clinical standard for evaluation of PS position and tissue recognition [9, 10]. But, it is not applicable as a real-time monitoring method during surgery. On the contrary, the X-ray fluoroscopy can achieve real-time monitoring [11–13], but the high radiation dose to surgeons and usually requiring multiple scans limit its use.

In previous studies, we have presented the design and implementation of the free-hand drilling probe as well as the spectrum measurement system for in vitro assessment of pattern from the optical reflectance [14, 15]. Based on this device, we have found some ways to explore the different tissues of porcine vertebrae on the PS fixation trajectory, by comparing the specific area and the peak value of reflected spectrums. However, these methods have some disadvantages, which cannot be avoided. In this paper, the spare representation-based classifier (SRC) was first applied for tissue optical reflectance spectra recognition [16]. Compared with other methods, the proposed method does not need to extract the features of area, peak, and shape of the spectra. Therefore, the computing complexity was reduced and the robustness and the real-time performance of the automatic identification were improved.

Recently, SRC was first proposed in 2008 and has been applied to face recognition and further extended to cancer classification [17–19]. SRC has been deeply studied by Yang et al. and some theoretical supports were provided for its

effectiveness [20]. A new SRC method was proposed by Peng et al., and a better representation coefficient vector was obtained [21]. Later, the SRC-steered discriminative projection (SRC-DP) method has been proposed for classification [22]. They have demonstrated that SRC can well characterize the local relationship of data. Later, the adaptive class preserving representation for classification (ACPRC) was proposed based on SRC [23]. However, SRC constructs all training images into a redundant dictionary, and the size of the redundant dictionary is very large, which makes the sparse solution of SRC time-consuming. Considering the large amount of spectral data, sparse preserving projection (SPP) was applied to improve the performance of SRC [24, 25], which was proposed by Qiao, and it has higher classification accuracy than PCA and NPE [26]. Sun et al. studied a novel supervised learning way, named supervised sparsity preserving projections (SSPP) and used it in face recognition [27].

Inspired by these meaningful works, we proposed a vertebral spectral data classification algorithm by combining SPP for dimensionality reduction and SRC for tissue recognition. Specifically, the spectra from various animal vertebral bones at similar positions along the trajectory were investigated, including fresh porcine vertebrae, bovine vertebrae, and ovine vertebrae. The same anatomical vertebral regions showed similar reflectance spectra among different animals. Then, the SPP method was used to reduce the dimension of spectra, and SRC was used for different animal vertebrae recognition along the fixation trajectory of PS. At last, other classification methods were applied and compared with our method. To our knowledge, this is the first report of a simple, accurate, and sensitive method based on the optical reflectance spectrum collected by the spectrum measurement system to monitor the PS during fixation.

2. Materials and Methods

2.1. Instrument. The experimental system for spectrum measurement is shown in Figure 1, which consists of a HL2000-HP-FHSA light source (Ocean Optics), free-hand drilling probe, USB2000 fibre optic spectrometer (Ocean Optics, wavelength gating from 200 nm to 1100 nm), and a computing workstation [16]. The self-made free-hand drill probe holder has a diameter of 5 mm, and two optical fibres with a diameter of 200 μm each were used for optical transmission and acquisition, respectively.

Data acquisition, scan conversion, and display were executed in real time at 2 frames per second in commercial LabVIEW interface software (National Instrument, Austin, TX). Each measurement showed the optical reflection spectrum with the wavelength range of 200–1100 nm. It was analysed by using customized software in LabVIEW and Matlab (Math Works, Natick, MA).

In the calculation of spectrum, the original spectrum was calibrated as $R = (\text{raw-dark})/(\text{reference-dark})$. Reference optical reflectance data were taken from a standard reflectance board (WS-1, Ocean Optics, Inc., Dunedin, FL), while the source light was on. The default assumption of the board was that the reference was equal to exactly 100% reflection in the wavelength range of 250–2500 nm. Dark optical reflectance signal due to random noise of the system was presented by turning off all the lights and covering the whole model. Raw optical reflectance data were obtained by placing OHDP on the surface of the vertebral bone. The background signal was subtracted from the actual measurement raw and reference spectra.

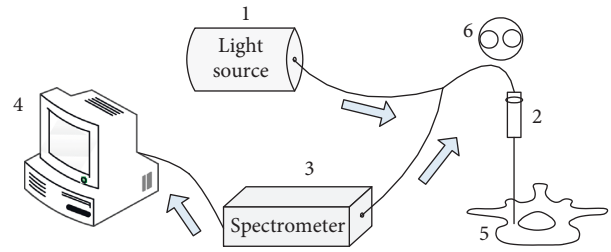

Figure 1: Schematic representation of the measurement system for the measuring spectrum on the vertebra bone model: 1, light source; 2, free-hand drilling probe; 3, CCD spectrometer; 4, computer; 5, porcine vertebra bone model; and 6, cross section of the probe.

2.2. Vertebral Bones Experiment. The human vertebra was similar to that of porcine, especially between T6 and T10 [25, 26]. We chose porcine vertebrae for this experiment. In this study, 10 fresh mature porcine vertebral bones weighting 38–45 kg were used. All vertebral bones were carefully cleaned off all soft tissues, except the periosteum, as shown in Figure 2.

Briefly, the light spectra were produced in a three-step process: first, porcine vertebra specimens were cut into two halves from the axial plane. The preferred trajectory of PS was drawn on the surface of the section of porcine vertebra. The length of the trajectory ranged from 22 to 35 mm. Nine sampling points were drawn on the trajectory line. The distance between them was 5 mm. Second, the optic probe was put on each sampling point, as shown in Figure 2(b). In order to eliminate the volatility, 30 spectra were recorded and stored for each point. Integrating time was 100 ms, and each optical reflectance spectra consisted of 2048 pixels.

In the bovine vertebra experiment, 10 fresh mature bovine vertebral bones weighting 300–350 kg were used. All vertebral bones were carefully cleaned. The light spectra were produced in a three-step process, which was similar to the steps in the porcine vertebra experiment. Several sampling points were chosen with an 8 mm distance between each two of them, due to the larger volume of bovine vertebra.

Ovine vertebra experiment also contained 10 fresh mature ovine vertebral bones weighting 70–80 kg. The vertebral bones were carefully cleaned off all soft tissues, as shown in Figure 2(e). The volume of ovine vertebra is smaller than that of porcine and bovine vertebrae. Therefore, the chosen sampling points have the nearest distance between each two of them. Other experimental steps were similar to those of porcine vertebrae experiments.

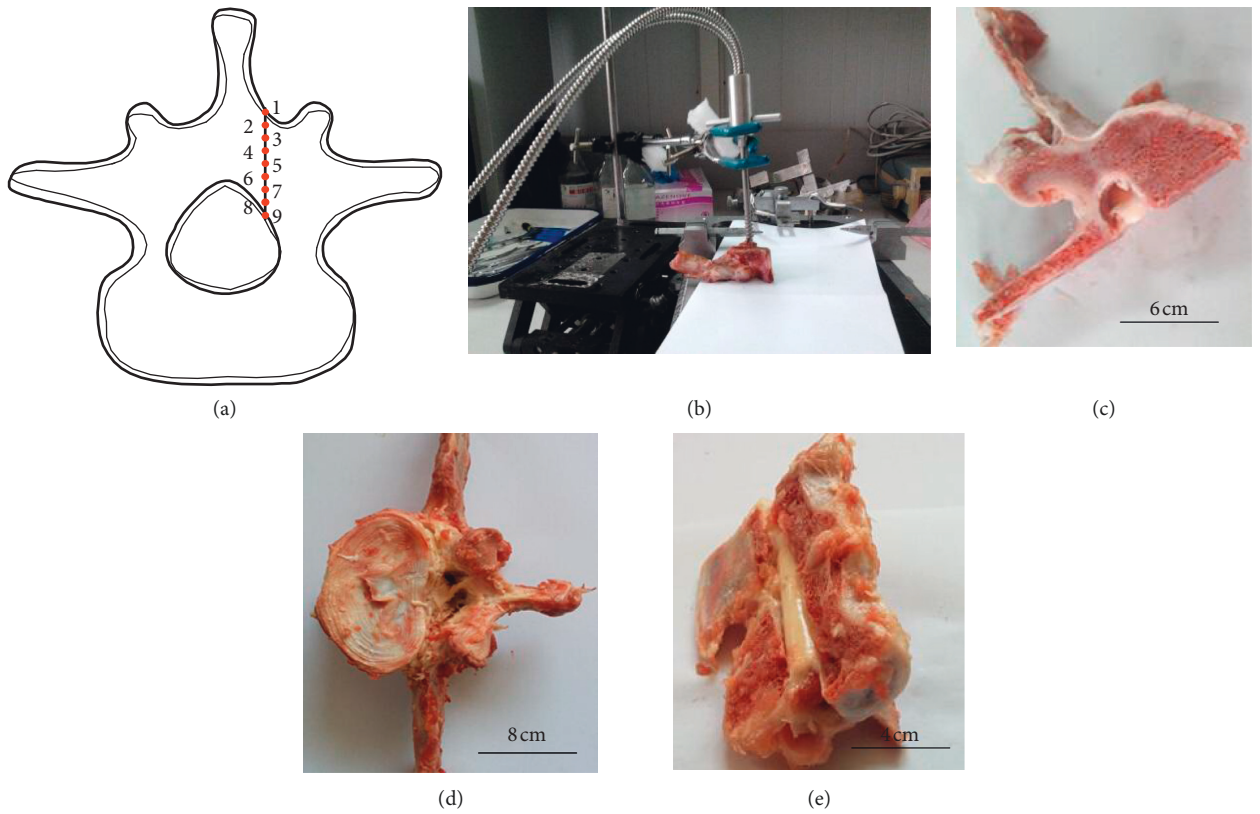

Figure 2: Photography of the experiment: (a) the diagram of animal vertebra, (b) photography of experiment, (c) porcine vertebra, (d) bovine vertebra, and (e) ovine vertebra.

Statistical analysis was carried out by the Student's t-test. In order to determine the significance of the differences between two groups, 95% confidence level was chosen. If the P value is less than 0.05, it is a significant difference.

2.3. Classification Method Based on the SRC. After the vertebra vector was obtained and normalized, SRC was used to distinguish different bone tissues. Based on this algorithm, SPP constructed an adjacent data set weight matrix and then projected the samples to a low-dimensional subspace with the reconstructive relationship best preserved. Here, we briefly describe the SRC algorithm for classification and SPP algorithm for data dimensionality reduction.

Suppose that $X = [x_1, x_2, \ldots, x_c] \in R^{m \times n}$ is regarded as a training sample set, where c refers to subclasses number, m denotes dimensionality, and n denotes the sample number. The i^{th} class training samples X_i can be used as $X_i = [x_{i1}, x_{i2}, \ldots, x_{in_i}] \in R^{m \times n}$ and $i = 1, 2, 3, \ldots, c$, where $X_{i,j}$ denotes a sample of i^{th} class and n_j corresponds to the i^{th} class training samples number. $y \in R^m$ refers to one of the test samples. Finally, the SRC problem can be shown in the following equation:

$$\delta(\phi) = \arg\min_{\phi} \left\{ \|y - X\phi\|_2^2 + \lambda \|\phi\|_1 \right\}, \tag{1}$$

where $\delta(\varphi)$ contains the SR coefficient of y with respect to X, and λ denotes a small positive constant. Then, to test sample y, we assign a label based on the SRC method as shown in the following equation:

$$e_i = \|y - X_i \delta_i(\varphi)\|_2^2, \tag{2}$$

where $\delta_i(\varphi)$ denotes the SR coefficient subvector associated with subclass X_i. The classification rule is set in the following equation:

$$\text{identity}(y) = \arg\min_i \{e_i\}. \tag{3}$$

Based on the abovementioned discussion, we summarize the SRC algorithm as follows:

Step 1. Normalize the columns of X to have unit l_2-norm and code y over X via l_1-minimization using equation (1)

Step 2. Compute the residuals e_i according to equation (2)

Step 3. Output the identity of y using equation (3)

Suppose $X = [x_1, x_2, \ldots, x_c] \in R^{m \times n}$ is the training sample set, c refers to the subclasses number, m is dimensionality, and n is the samples number. First, the version of SPP obtains a SR coefficient vector for each sample X_i by solving a modified l_1 problem:

$$\begin{aligned} \min_{\theta_i} \quad & \|\theta_i\|_1 \\ \text{s.t.} \quad & \|x_i - X_i\theta_i\| < \varepsilon, \\ & I = I^T\theta_i, \end{aligned} \tag{4}$$

where $\theta_i = [\theta_{i1}, \ldots, \theta_{i,i-1}, \theta_{i,i+1}, \ldots, \theta_{in}]^T \in R^n$ is the n-dimensional coefficient vector in which the i^{th} element equals

to zero (implying X_i is removed from X) and ε is the residual constraint value. All optimal sparse reconstruction coefficient vectors $\widehat{\theta}_i$ are from a sparse weight matrix $\widehat{\theta}_i = [\theta_1, \ldots, \theta_i, \ldots, \theta_n]^T \in R^{n\times n}$, which characterizes the sparse reconstructive relationship among samples.

Second, SPP seeks the projections, which makes preservation of the sparse reconstructive relationship best, by solving the following optimization problem:

$$\min_P \sum_{i=1}^{n} \left\| P^T x_i - P^T X \widehat{\theta}_i \right\|^2, \tag{5}$$

where X is a matrix dictionary for all training samples and $P \in R^{m\times d}$ is the projection matrix. The problem of equation (5) can be solved based on the following equation:

$$X\left(\theta + \theta^T - \theta^T\theta\right)X^T p = \lambda X X^T p. \tag{6}$$

The projection matrix is composed of the eigenvectors corresponding to the largest d eigenvalues in the selection equation (6). Then, the training samples and the test samples both are projected on the projection matrix in order to reduce the dimension, and finally the classification and recognition are carried out.

Based on the above mentioned discussion, we summarize the SPP algorithm as follows:

Step 1. Construct weight matrix θ using equation (4).

Step 2. Calculate the projection vectors P according to equation (6). Also, the eigenvectors corresponding to the largest d eigenvalues span the optimal subspace.

3. Results

The classification of various vertebral tissues based on SRC and SPP algorithm is proposed in this paper. To verify the effectiveness of this algorithm, the proposed algorithm is compared with other algorithms. First, recognition accuracy of different spectral data based on the same animal or tissue was compared. Second, SPP was used as a preprocessor for any typical classifiers, including SRC, SVM, and 1NN. Recognition accuracy based on different classifiers was compared. The experimental samples were tested in Matlab 2013a and run on a PC (2.50 GHz CPU, Intel Core2 Duo, 2 GB RAM).

3.1. Original Spectrum. Figure 3 shows a representation of spectra relating to 9 sampling points along the trajectory from one bone of each of the three animal species after pretreatment. Each spectrum curve represents the value in one sampling point on one animal vertebra. Point 1 and point 9 are in the cortical bones, and points 2 to 8 are in the cancellous bones. The values of point 1 and point 9 in cortical bones are both distinct from those in the cancellous bones. The values of point 1 and 9 are larger than those of points 2 to 8 in Figure 3(a). However, the values of point 1 and 9 are smaller than those of points 2 to 8 in Figures 3(b) and 3(c).

3.2. Results of Different Spectral Data Groups. In this paper, spectral database contains experimental data on vertebral tissue of three species of animals. Specifically, porcine vertebral data were defined as Group 1, bovine vertebral data were defined as Group 2, and ovine vertebral data were defined as Group 3. Each group contains 80 samples, and each sample contains 10 spectra. In addition, cortical bone data were defined as Group A, and cancellous bone data were defined as Group B. Each group contains 120 samples, and each sample contains 10 spectra. A total of five experimental groups were used as the input of the classifier after data dimension reduction. The experimental group contains 40 samples, such as Group 1A and Group 1B, and each sample contains 10 spectra.

In each experiment, half of the samples were used for training, and the remaining were used as testing samples. The experiment was repeated 10 times. The recognition accuracy was calculated, as shown in Table 1. For different experimental groups, the recognition rate was different.

3.3. Results Based on Different Classifiers. In this experiment, different classifiers were applied, including SPP + SRC, SPP + 1NN, and SPP + SVM, and three experimental groups were used as input of these classifiers. The experimental group contains 80 samples, such as Group 1 and Group 2, and each sample contains 10 spectra. Half of the samples were selected for training, and the remaining samples were used for testing in each experiment. The experiment was repeated 10 times. The average recognition accuracy was calculated, as shown in Table 2. The recognition rate of the proposed algorithm was higher than that with other algorithms.

4. Discussion

In PS fixation, there are two major problems to the effect of surgery [28]. The first one is that the tip of the traditional instrument breaks the boundary of the bone (cortical bone) and damages ambient organs of patients. The second one is that the screw is not placed in the exact position and the fixation stability is not strong. The ideal position is approached by that the screw is placed through the arch of the cancellous bone till the tip arrives at the cortical bone. In the previous study, the method based on optical spectrum and needle-like probe presented a new way to overcome the two problems to the most extent, which was working on the principle of the local bone reflectance spectrum.

In this study, different animal bones were used in the experiment, including porcine vertebra, bovine vertebra, and ovine vertebra. The measurement device was put on the section surface to obtain the original spectrum. We obtained different animal vertebral spectra according to 9 sampling points along the trajectory. In Figure 3, each spectrum curve represents a different sampling point on one animal vertebra. Point 1 and point 9 are in the cortical bones and points 2 to 8 are in the cancellous bones. The results show that the values of point 1 and point 9 in cortical bones are both distinct from those in the cancellous bones. During different

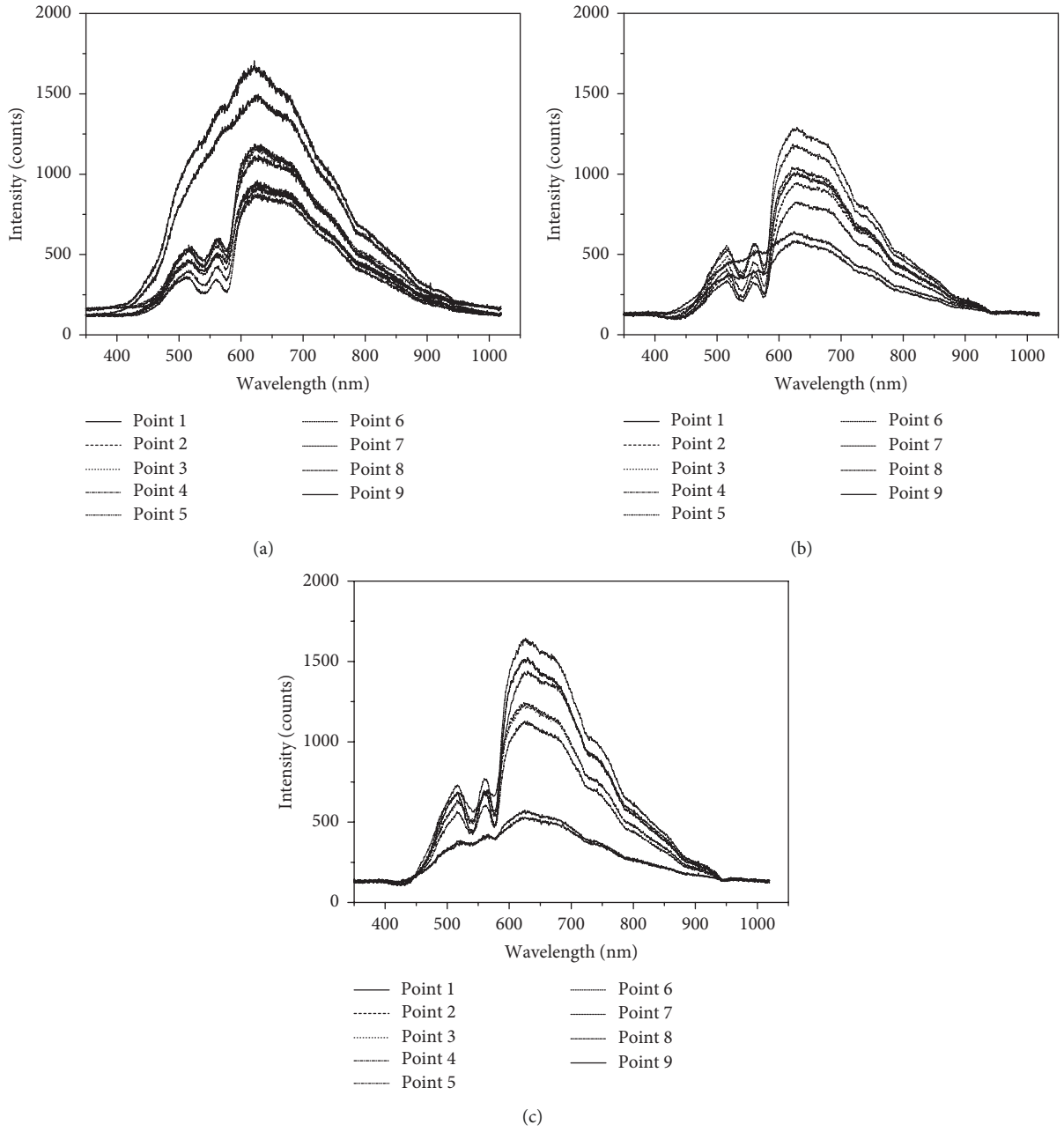

Figure 3: Original spectra from the vertebra of different animal species: (a) original spectra of one porcine vertebra, (b) original spectra of one bovine vertebra, and (c) original spectra of one ovine vertebra.

animal experiment, the values of point 1 and 9 are compared with those of points 2 to 8. We found that some values of point 1 and 9 are larger but some are not. It means the spectra of cancellous bones and cortical bones have similar shapes but different values. The cause of this result is that different vertebrae have different structures. It is the first time to search for differences in vertebral spectra among different animal species.

In this study, near-infrared optical spectroscopy was used, which would not be the only way. Another optical spectroscopy has also been used in both clinical and basic research about vertebra [29]. For example, the cartilage, subchondral bone, and cancellous bone could be examined by using a fibre-optic Raman spectroscope. As reported in the literature, the varying optical signal can provide some information about structures and composition of bone, such as bone mineral crystallinity and tissue density. In this study, the cortical and cancellous bones are different in mineral crystallinity and density. The near-infrared optical spectrum will be characterized according to different domains in different animal experiments.

In the classification part, different vertebral tissues identification methods based on SPP algorithm are proposed. The research shows that if SRC is used, the

Table 1: The average recognition rates of SRC and SPP algorithm based on different groups.

Group	1A and 1B	2A and 2B	3A and 3B	1A, 2A, and 3A	1B, 2B, and 3B
Average recognition rate (%)	86	83	85	81	80
Standard deviation	±1.6	±1.5	±1.5	±1.3	±1.5

Table 2: The recognition rates of different algorithms.

Group	Recognition rates	1A, 2A, and 3A	1B, 2B, and 3B
SPP + SRC	Average recognition rate	81%	80%
	Standard deviation	±1.3	±1.5
SPP + 1NN	Average recognition rate	73%	72%
	Standard deviation	±2.1	±1.7
SPP + SVM	Average recognition rate	76%	74%
	Standard deviation	±0.9	±1.1

classification performance of the most significant feature will converge with the increase in feature dimension [30, 31]. Even so, effective feature extraction is still very important because classification algorithms can become simple and easy to handle. For practical spectral data recognition, a small amount of representation features is desirable, because it can reduce storage requirements and improve classification efficiency. Therefore, SPP is used to implement a small number of presentation features to achieve better performance [32]. The algorithm first constructs the adjacency weight matrix of the data set based on an improved SR framework and then evaluates the low-dimensional embedding of data to keep the weight matrix optimal. Though SPP is essentially a global method, it has some local properties because of its sparse representation process, as shown in the experimental results.

A good method should be applied on the large accuracy data based on fact verification. First, different spectral data groups were input to the classifier, and the results are shown in Table 1. Based on the same classification method, cortical bones and cancellous bones of porcine vertebrae (Group 1A and 1B) have the highest recognition rate and cortical bones and cancellous bones of bovine vertebrae (Group 3A and 3B) have the lowest recognition rate. These results suggest that cortical bones and cancellous bones of porcine vertebrae are quite different based on the spectrum. The result of this experiment may suggest that the porcine vertebrae have stable bone structure and large bone structural differences. Moreover, the recognition rate of three animal cortical bones (Group 1A, 2A and 3A) is higher than that of three animal cancellous bones (Group 1B, 2B, and 3B). These results suggest that there is little difference in the same type of bone structure for different animal species and structural differences in cancellous bones are smaller.

Second, different algorithms based on SPP were used to identify different tissues in porcine, bovine, and ovine vertebral bones. Compared with the 1NN and SVM classifier, SRC based on the proposed method performs better during tissue classification. The comparison of classification accuracy of our results with the previous works is given in Table 2. The experimental results indicate that the average accuracy rate achieved by the proposed method is 86%, which is higher than that from other methods. Our results suggest that SRC solves the influence of external interference factors on recognition, enhances the robustness of recognition, and improves the recognition rate. In addition, PCA and NPE were used as different data dimension reduction methods in this paper. The results show that SPP can be more conveniently used in practice and has higher accuracy with SRC (average recognition rate of PCA + SRC was 75% and that of NPE + SRC was 75%), which are in good agreement with [33].

This paper provides a vertebral tissue classification method for assisting the surgical procedure. This method can effectively distinguish different tissues along the PS implant path, and it can also distinguish different animal bone tissues. However, each approach has its own advantages and plays out differently in different situations. For application, the method must have high sensitivity, should be in real time, and be accurate. There are two things one should do to validate and verify this method: first, the sample number needs to be increased and more calculation methods are needed to be improved and tested; second, the surgery required real-time and accurate acquisition. In the follow-up work, we will try to overcome these limitations by using other detection methods and integrate relevant information into classification or dimension reduction algorithm to improve its performance.

5. Conclusions

In this study, a NIRs optical fibre probe is employed to monitor the tissues characteristic spectrum along the PS placement trajectory in various animal vertebral bones. Then, we investigated the near infrared spectroscopy and distinguished different tissues along the fixation trajectory of PS based on SRC. The main research contents of this project include the following:

(1) We measured the spectrum of tissue on the trajectory of the pedicle screw. Fresh porcine vertebrae, bovine vertebrae, and ovine vertebrae were used in the experiments.

(2) The proposed method based on the SPP method for dimensionality reduction and the SRC method for tissue recognition was used in vertebra classification and showed superior performance.

The results gained from this project are vital significant to the development of hi-tech medical instruments with independent intellectual property rights.

Data Availability

The spectrum data used to support the findings of this study are partly included within the supplementary information files. The research based on these data is still underway, and all the spectrum data cannot be disclosed until the research is completed.

Conflicts of Interest

The authors declare that there are no conflicts of interest regarding the publication of this paper.

Acknowledgments

This work was supported by Nanjing Institute of Technology high level introduction of talents Research Fund (YKJ201862 and YKT201866), National Major Scientific Instruments and Equipment Development Project Funded by National Natural Science Foundation of China (81827803 and 81727804), National Natural Science Foundation of China (61875085 and 81601532), Natural Science Foundation of Jiangsu Province (BK20160814), and Jiangsu Science and Technology Support Plan (Social Development) (BE2016759).

Supplementary Materials

These data are divided into six groups. Specifically, porcine vertebral data were defined as Group 1, bovine vertebral data were defined as Group 2, and ovine vertebral data were defined as Group 3. In addition, cortical bone data were defined as Group A and cancellous bones data were defined as Group B. (*Supplementary Materials*)

References

[1] J. M. Diniz and R. V. Botelho, "Is fusion necessary for thoracolumbar burst fracture treated with spinal fixation? a systematic review and meta-analysis," *Journal of Neurosurgery Spine*, vol. 27, no. 5, pp. 1–9, 2017.

[2] K. Matsukawa, Y. Yato, R. A. Hynes et al., "Cortical bone trajectory for thoracic pedicle screws: a technical note," *Clinical Spine Surgery*, vol. 30, no. 5, pp. 497–504, 2017.

[3] O. L. Ulusoy, S. Kahraman, I. Karalok et al., "Pulmonary cement embolism following cement-augmented fenestrated pedicle screw fixation in adult spinal deformity patients with severe osteoporosis (analysis of 2978 fenestrated screws)," *European Spine Journal*, vol. 27, no. 9, pp. 2348–2356, 2018.

[4] K. Panagiotis, M. Eva, S. Vasileios et al., "Percutaneous injection of strontium containing hydroxyapatite versus polymethacrylate plus short-segment pedicle screw fixation for traumatic A2- and A3/AO-type fractures in adults," *Advances in Orthopedics*, vol. 2018, Article ID 6365472, 8 pages, 2018.

[5] A. H. S. Al, M. A. Sabbahi, H. N. Alrowayeh et al., "Electromyographic activity of quadriceps muscle during sit-to-stand in patients with unilateral knee osteoarthritis," *BMC Research Notes*, vol. 11, no. 1, pp. 356–361, 2018.

[6] J. M. Beckman, G. Murray, K. Bach, A. Deukmedjian, and J. S. Uribe, "Percutaneous minimally invasive (mis) guide wire-less self-tapping pedicle screw placement in the thoracic and lumbar spine: safety and initial clinical experience: technical note," *Operative Neurosurgery*, vol. 11, no. 4, pp. 530–536, 2015.

[7] I. Saarenpää, T. Laine, J. Hirvonen, J. Hirvonen et al., "Accuracy of 837 pedicle screw positions in degenerative lumbar spine with conventional open surgery evaluated by computed tomography," *Acta Neurochirurgica*, vol. 159, no. 10, pp. 2011–2017, 2017.

[8] J. N. Weinstein, K. F. Spratt, D. Spengler, C. Brick, and S. Reid, "Spinal pedicle fixation: reliability and validity of roentgenogram-based assessment and surgical factors on successful screw placement," *Spine*, vol. 13, no. 9, pp. 1012–1018, 1988.

[9] A. F. Jr, T. L. Thompson, S. Campbell et al., "Use of intraoperative isocentric c-arm 3d fluoroscopy for sextant percutaneous pedicle screw placement: case report and review of the literature," *The Spine Journal*, vol. 5, no. 3, pp. 339–343, 2005.

[10] S. Rajasekaran, S. Vidyadhara, and A. Shetty, "Intra-operative iso-c3d navigation for pedicle screw instrumentation of hangman's fracture: a case report," *Journal of Orthopaedic Surgery*, vol. 15, no. 1, pp. 73–77, 2007.

[11] K. Kotil and T. Bilge, "Accuracy of pedicle and mass screw placement in the spine without using fluoroscopy: a prospective clinical study," *The Spine Journal*, vol. 8, no. 4, pp. 591–596, 2008.

[12] B. G. Ochs, C. Gonser, T. Shiozawa et al., "Computer-assisted periacetabular screw placement: comparison of different fluoroscopy-based navigation procedures with conventional technique," *Injury*, vol. 41, no. 12, pp. 1297–1305, 2010.

[13] A. Onibokun, L. T. Khoo, and S. Bistazzoni, "Anatomical considerations for cervical pedicle screw insertion: the use of multiplanar computerized tomography measurements in 122 consecutive clinical cases," *Spine Journal*, vol. 9, no. 49, pp. 729–734, 2009.

[14] W. Li, Y. Liu, H. Sun et al., "Monitoring reduced scattering coefficient in pedicle screw insertion trajectory using near-infrared spectroscopy," *Medical & Biological Engineering & Computing*, vol. 54, no. 10, pp. 1–7, 2015.

[15] W. Li, Y. Liu, and Z. Qian, "Determination of detection depth of optical probe in pedicle screw measurement device," *BioMedical Engineering OnLine*, vol. 13, no. 1, pp. 148–160, 2014.

[16] C. Weaver and N. Saito, "Improving sparse representation-based classification using local principal component analysis," *Computational Intelligence for Pattern Recognition*, vol. 777, pp. 165–206, 2018.

[17] J. Wright, "Robust face recognition via sparse representation," *IEEE Transactions on Pattern Analysis and Machine Intelligence*, vol. 31, no. 2, pp. 210–227, 2008.

[18] J. Wen, Y. Xu, Z. Li, Z. Ma, and Y. Xu, "Inter-class sparsity based discriminative least square regression," *Neural Networks*, vol. 102, pp. 36–47, 2018.

[19] T. Liu, J.-X. Mi, Y. Liu, and C. Li, "Robust face recognition via sparse boosting representation," *Neurocomputing*, vol. 214, no. 2, pp. 944–957, 2016.

[20] J. Yang, L. Zhang, Y. Xu, and J.-Y. Yang, "Beyond sparsity: the role of L1-optimizer in pattern classification," *Pattern Recognition*, vol. 45, no. 3, pp. 1104–1118, 2012.

[21] P. Yali, L. Lingjun, L. Shigang et al., "Extended sparse representation-based classification method for face recognition," *Machine Vision and Applications*, vol. 29, no. 6, pp. 991–1007, 2018.

[22] J. Yang, D. Chu, L. Zhang, Y. Xu, and J. Yang, "Sparse representation classifier steered discriminative projection with applications to face recognition," *IEEE Transactions on*

Neural Networks and Learning Systems, vol. 24, no. 7, pp. 1023–1035, 2013.

[23] J. Mi, Q. Fu, and W. Li, "Adaptive class preserving representation for image classification," in *Proceedings of the 2017 IEEE Conference on Computer Vision and Pattern Recognition (CVPR)*, Honolulu, HI, USA, July 2017.

[24] Y. Wang, H. Zhang, and F. Yang, "A weighted sparse neighbourhood-preserving projections for face recognition," *IETE Journal of Research*, vol. 63, no. 3, pp. 1–10, 2017.

[25] Z. Wei, K. Peipei, F. Xiaozhao et al., "Joint sparse representation and locality preserving projection for feature extraction," *International Journal of Machine Learning and Cybernetics*, vol. 10, no. 7, pp. 1731–1745, 2019.

[26] L. Qiao, S. Chen, and X. Tan, "Sparsity preserving projections with applications to face recognition," *Pattern Recognition*, vol. 43, no. 1, pp. 331–341, 2010.

[27] Y. Sun, J. Zhao, and Y. Hu, "Supervised sparsity preserving projections for face recognition," *Proceedings of SPIE*, vol. 8009, no. 4, pp. 357–366, 2011.

[28] T. M. Heintel, S. Dannigkeit, A. Fenwick et al., "How safe is minimally invasive pedicle screw placement for treatment of thoracolumbar spine fractures?" *European Spine Journal*, vol. 26, no. 5, pp. 1–10, 2016.

[29] C. D. C. A. Lopes, P. H. J. O. Limirio, V. R. Novais et al., "Fourier transform infrared spectroscopy (FTIR) application chemical characterization of enamel, dentin and bone," *Applied Spectroscopy Reviews*, vol. 53, no. 3, pp. 1–23, 2018.

[30] X. Tang, G. Feng, and J. Cai, "Weighted group sparse representation for undersampled face recognition," *Neurocomputing*, vol. 145, pp. 402–415, 2014.

[31] Y. Xu, Z. Zhong, J. Yang, J. You, and D. Zhang, "A new discriminative sparse representation method for robust face recognition via l_{2} regularization," *IEEE Transactions on Neural Networks and Learning Systems*, vol. 28, no. 10, pp. 2233–2242, 2017.

[32] Z. Pan, Z. Deng, Y. Wang, and Y. Zhang, "Dimensionality reduction via kernel sparse representation," *Frontiers of Computer Science*, vol. 8, no. 5, pp. 807–815, 2014.

[33] Q. Lishan, S. Chen, and X. Tan, *Sparsity Preserving Projections with Applications to Face Recognition*, Elsevier Science Inc., Amsterdam, Netherlands, 2010.